JOURNAL OF MATERIALS SCIENCE 31 (1996) 6251–6257

Preparation of nanocomposite materials containing WS_2, δ-WN, Fe_3O_4, or Fe_9S_{10} in a silica aerogel host

M. R. AYERS, X. Y. SONG, A. J. HUNT
Energy and Environment Division, Earnest Orlando Lawrence Berkeley National Laboratory, University of California, Berkeley, CA 94720 USA

Nanocomposite materials based on silica aerogel hosts have been produced using chemical vapour infiltration/decomposition methods and characterized by X-ray diffraction and electron microscopy. Amorphous tungsten in SiO_2 aerogel was formed by the decomposition of $W(CO)_6$ at 250 °C. Alternatively, reaction of this material with sulphur at 700 °C produced needle-shaped WS_2 crystals with lengths ranging from 25–230 nm. Reaction of the W/SiO_2 composite with anhydrous NH_3 formed crystals of δ-WN with diameters of 1–5 nm. $Fe(CO)_5$ is readily absorbed into the silica aerogel, forming an amorphous iron oxide/SiO_2 composite after slow oxidation in air. Treatment of this material with additional $Fe(CO)_5$ produced an Fe_3O_4/SiO_2 aerogel composite. Fe_3O_4 particle sizes were 20–55 nm. After additional heat treatment, this composite exhibited soft ferromagnetic behaviour with a coercivity of ~170 Oe. Fe_9S_{10} crystals with diameters of 30–90 nm were formed by the reaction of the amorphous iron oxide/SiO_2 composite with H_2S at 900 °C.

1. Introduction

Composite materials where the primary features of either the host or the guest phase possess dimensions on the order of 1–100 nm are termed "nanocomposites." Desirable characteristics for the guest phase of a nanocomposite material include, small particle size, narrow particle-size distribution, and a uniform dispersion of particles throughout the host matrix. Control of these features can lead to enhanced physical properties such as non-linear optical behaviour [1], super paramagnetism or superferromagnetism [2, 3], giant magnetoresistance [4] and catalytic activity [5–7]. Ideally, the host material would permit the preparation of composites with a range of host to guest ratios and guest morphologies by simply varying the experimental conditions.

Silica aerogels and xerogels, prepared by well-developed sol–gel chemistry, retain many advantageous qualities for nanocomposite host materials. For aerogels, these include, ease of preparation, high surface areas, high permeability, good thermal resistance, and reasonable chemical inertness. Breitscheidel *et al.* [8], and Lukehart *et al.* [9], have successfully prepared nanocomposites of various inorganic phases in silica xerogels. These preparations involved the addition of an inorganic precursor to a sol that contained either a prescribed amount of an alkoxysilane containing a chelating group or a bifunctional chelating group engineered directly into the primary alkoxide precursor. However, contamination by remnants of the coupling agent, or rapid decomposition of the inorganic precursor in the sol, could introduce experimental limitations for certain guest compositions.

An alternative method leading to nancomposite materials utilizes chemical vapour infiltration (CVI) to deposit a volatile inorganic compound within a silica aerogel host. The extremely high porosity of silica aerogels (95%–99%) often allows the guest species to deposit uniformly throughout a monolithic aerogel sample. Once deposited, thermal, photolytic, or chemical treatment can easily produce the desired product. This report describes the preparation and properties of nanocomposites based on a silica aerogel and containing WS_2, δ-WN, Fe_3O_4, and Fe_9S_{10}.

2. Experimental procedure

2.1. General procedures

Monolithic silica aerogels were prepared by a two-step acid–base catalysed process using commercially obtained precondensed tetraethylorthosilicate as the silica source (Silbond Chemical; Silbond H-5). The volume ratios of precondensed silica/ethanol/water/30% NH_4OH were typically $1.0/1.67/1.5/6.7 \times 10^{-3}$. After gelation, samples were aged in a 70% ethanol/30% water solution at a pH of 8.5 for at least 48 h. Further soaking in pure ethanol removed the water contained within the alcogels. Solvent exchange with CO_2 and supercritical drying followed previously reported procedures [10]. Typically, aerogels prepared in this way had an apparent density of 0.05–0.10 $g\,cm^{-3}$ and a single-point nitrogen BET surface area of 800–900 $m^2\,g^{-1}$.

0022–2461

Iron pentacarbonyl and tungsten hexacarbonyl were obtained from Aldrich Chemical Co. and were used without further purification. Anhydrous NH_3 was purchased from Matheson Gas Products with a purity of 99.99% and was used as-received.

Transmission electron micrographs were recorded using a JEM-200CX, a JEM-200CX-AEM, or a TOPCON-002B each operating at 200 kV. Sample preparation for high-resolution transmission electron microscopy (HRTEM) involved grinding the samples to fine powders in acetone and evaporating the resulting suspensions on to copper grids coated with a holey carbon film. X-ray diffraction (XRD) powder patterns were obtained on a Siemens Kristalloflex diffractometer using CuK_α radiation. Crystalline phases were identified by comparison with literature patterns [11]. Infrared spectra were acquired using KBr pellets of powdered samples on a Perkin–Elmer 710B spectrophotometer. Magnetization curve measurements utilized an EGG 4500 vibrating sample magnetometer, calibrated against a cylindrical nickel standard.

2.2. Deposition of amorphous tungsten in a silica aerogel

A monolithic piece of silica aerogel less than 10 cm^3 in size was placed in a wide-mouth Schlenk flask containing 0.20–0.30 g $W(CO)_6$. The vessel was slowly evacuated and refilled with dry argon several times. The flask was tightly secured and placed in an oven maintained at 120 °C for 18 h. Upon removal, the sample possessed a faint brown colour. During cooling, microcrystals of $W(CO)_6$ formed throughout the entire volume of the aerogel. The sample was then removed, placed in a tube furnace under a 300 ml min^{-1} flow of argon, quickly heated to 300 °C, and held at that temperature for 30 min. Small amounts of $W(CO)_6$ collected at the outlet of the tube. Upon removal, the sample was uniformly black in appearance and had retained its original shape. Typical mass gains ranged from 3%–5%; however, this process could be repeated several times on the same sample until any desired loading was achieved. Samples prepared in this way appeared to be air stable, but the deposited material could be completely removed by heating the sample above 250 °C in an oxidizing atmosphere, implying that the fine microstructure of the deposits leads to volatile oxidation products.

Electron microscopy revealed a high-contrast film spread throughout the aerogel host. The material did not diffract electrons or X-rays and did not crystallize after heating to 700 °C under argon for 12 h.

2.3. Preparation of WS_2/SiO_2 aerogel composites

A monolithic piece of tungsten-doped aerogel (0.25 g, 6% W wt/wt) was placed in a quartz boat within a tube furnace. A second boat containing 2.0 g sulphur and fitted with a magnetic push-bar was placed outside the furnace's hot zone. The sample was heated to 700 °C under flowing argon. The boat containing sulphur was then slid into the hot zone, and sulphur vapour was maintained above the sample for 1 h. The system was held at 700 °C for an additional 18 h. After cooling under argon, the sample had retained its shape but had changed from black to greenish-yellow. The overall mass gain relative to the pure silica aerogel was 8% (this and subsequent mass gain values are not corrected for water loss due to the condensation of surface hydroxyl group that occurs above 450 °C for silica aerogels).

2.4. Preparation of δ-WN/SiO_2 aerogel composites

A monolithic piece of tungsten-doped aerogel (0.64 g, 20% W wt/wt) was placed in a quartz boat within a tube furnace. The sample was heated to 600 °C under flowing argon at 200 ml min^{-1}. Hydrogen was then added to the gas stream at 200 ml min^{-1} to reduce any oxide present. After 2 h, the hydrogen flow was discontinued, and the temperature reduced to 480 °C. The atmosphere above the sample was then changed from argon to anhydrous NH_3 at 300 ml min^{-1}. The system was maintained under these conditions for 24 h and then cooled to room temperature under argon. The sample was uniformly black and had retained its original shape. The overall weight gain of the sample relative to the pure silica aerogel was 17%.

2.5. Deposition of amorphous iron oxide in silica aerogel

A monolithic piece of silica aerogel less than 10 cm^3 in size was placed in a wide-mouth Schlenk flask containing a bed of glass beads. The vessel was slowly evacuated and refilled with dry argon several times. Under a flow of argon, 0.10–0.20 ml $Fe(CO)_5$ was carefully added, such that the liquid was contained within the bead bed and did not contact the aerogel sample. The flask was tightly secured and placed in an oil bath maintained at 55 °C for 18 h. After several hours, the aerogel sample appeared transparent yellow–green. The flask was then removed from the oil bath, and the stopcock opened to air (samples prepared in this way were often pyrophoric if quickly exposed to air). As air diffused into the flask, the colour of the sample slowly changed to a dark orange–brown. The sample showed slight scaling of the top surface, but otherwise remained monolithic. After several hours, the sample was transferred to a furnace and heated to 350 °C for 18 h. Electron microscopy revealed a high-contrast film spread throughout the aerogel host. The material did not diffract electrons or X-rays and was assumed to contain both Fe_2O_3 and FeO(OH).

2.6. Preparation of Fe_3O_4/SiO_2 aerogel composites

A monolithic piece of iron oxide-doped aerogel (0.40 g) was placed in a wide-mouthed Schlenk flask as described above. The flask was charged with 0.20 ml $Fe(CO)_5$. The sample immediately began to change

from dark orange–brown to black. After 1 h, the stopcock was opened and air was allowed to diffuse slowly into the flask. After standing for 1 h, this process was repeated three times. The sample appeared black with a thin silvery layer on the top surface. Although considerably more fragile than pure aerogel, the sample remained monolithic. Annealing the sample at 720 °C for 18 h caused significant cracking and shrinkage. The overall weight gain relative to the pure silica aerogel was 35%.

2.7. Preparation of Fe_9S_{10}/SiO_2 aerogel composites

A monolithic piece of iron oxide-doped aerogel (0.35 g) was placed in tube furnace and heated to 900 °C under a 300 ml min^{-1} flow of argon. A flow of H_2S was added (generated from FeS + dilute HCl) and maintained for 3 h. A small amount of sulphur collected at the vent end of the tube. The system was held at 900 °C under argon for 18 h, and then cooled to room temperature. The sample had significantly cracked and shrunk and appeared black with a silvery microcrystalline layer on the top surface. The overall weight gain relative to the pure silica aerogel was 10%.

3. Results and discussion

Silica aerogels have many physical characteristics that make them attractive substrate materials for nanocomposites formed by CVI methods. The pore structure of aerogels consists of a random network of open micro-, meso-, and macropores. This allows facile transport of guest-phase precursors throughout the body of the gel during composite formation. The open pore structure would also improve performance, relative to xerogels, when the end use, or final processing, of the composite involves gas phase reactants. The silica surface of aerogel normally exhibits a moderate chemical activity [12]. However, if required, a deactivation step can eliminate this property. Adsorption of a second phase on the aerogel host can occur through a combination of chemisorption, micropore filling, capillary condensation and Lagmuir–BET surface adsorption [13]. For the latter three cases, the extent of loading depends on the partial pressure of the adsorbate. This gives a certain level of control of the mass fraction, and, concurrently, the particle size and dispersion of the guest phase.

Transition metal carbonyl complexes possess two very desirable attributes for a nanocomposite precursor. They decompose under relatively mild conditions, usually giving only their base metals and carbon monoxide. Additionally, many possess sufficient vapour pressure to fill an aerogel host through the vapour phase. The vapour pressure, p, of a guest precursor at an absolute temperature, T, can be found using

$$\ln(p) = \frac{-A}{T} + B \qquad (1)$$

For $W(CO)_6$, $A = 9489$ and $B = 33.3$ gives p (Pa) [14], while for $Fe(CO)_5$, $A = 4827.8$ and $B = 24.46$ [15] (modified from the literature to use SI units and natural logarithm).

The adsorption of $W(CO)_6$ in a silica aerogel proceeds in a straightforward manner. The relatively low vapour pressure of $W(CO)_6$ allows only small (< 5%) amounts of deposition. However, the process can be repeated several times to achieve any desired loading level. At 250 °C, decomposition to an amorphous material, presumed to be elemental tungsten, occurs. Electron microscopy did not reveal the presence of crystalline phases through visual inspection of the micrographs or by electron diffraction. EDS analysis showed only silicon, oxygen and tungsten, although this could not rule out the presence of WO_x or WC. The infrared spectra of $W(CO)_6$-filled SiO_2 aerogel and the same sample after heat treatment appear in Fig. 1. The spectrum of the sample before heat treatment shows a characteristic ν-CO vibration at 1980 cm^{-1}. The remaining bands in the spectrum result from Si–O–Si, – OH and adsorbed H_2O vibrations. The 250 °C spectrum shows only a trace of the ν-CO band. This material proved to be a useful starting point for further reactions.

Composites of the semiconductor WS_2 in silica aerogel formed through the reaction of the amorphous tungsten composite and sulphur vapour at 700 °C. Fig. 2 shows electron micrographs of the WS_2/SiO_2 aerogel composite. The WS_2 phase possessed a needle-like morphology, with lengths ranging from 25–230 nm (mean 65 nm, S.D. = 30 nm) and thicknesses of 1–15 nm (mean 4 nm, S.D. = 3 nm). The crystals were typically well formed, though a small number had significant defects, as shown in Fig. 2c. Tenne *et al.* have recently found fullerene-like structures of WS_2 formed by the reaction of tungsten film with H_2S [16, 17]. Interestingly, no similar structures were found here, perhaps due to reduced surface interaction between the growing WS_2 crystals and the highly porous silica host. Table I gives the X-ray diffraction results for the various SiO_2 nanocomposites. In all cases, the amorphous silica matrix strongly scattered radiation for 2θ from 0° to 45°, interfering with the observance of low θ reflections.

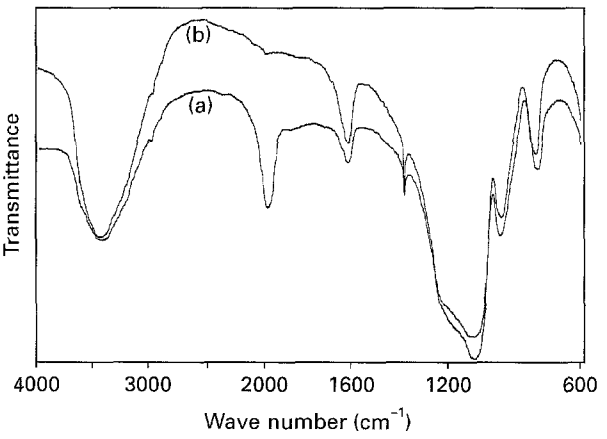

Figure 1 Infrared spectra of (a) silica aerogel doped with $W(CO)_6$, and (b) the same sample after thermal decomposition at 250 °C under argon.

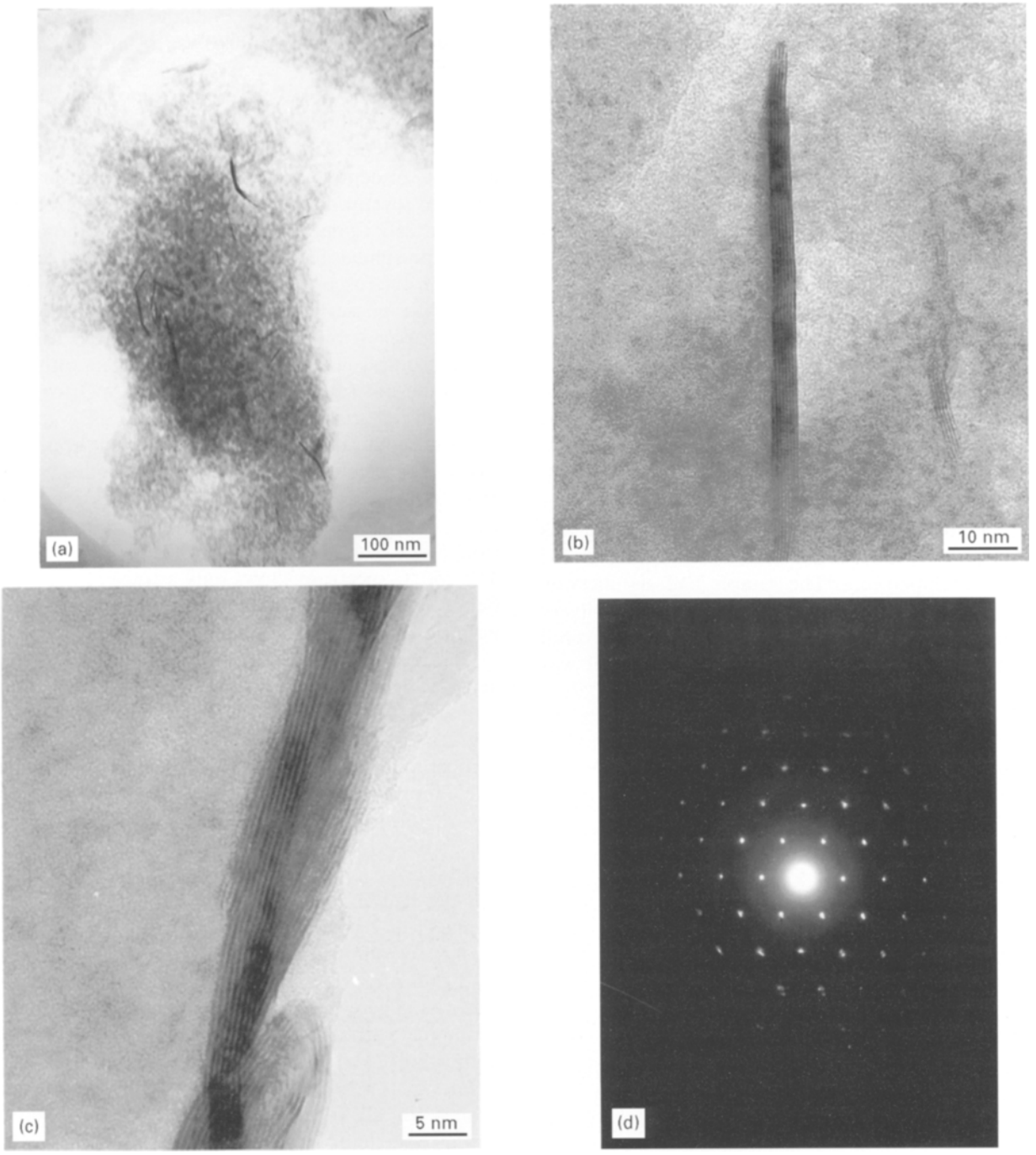

Figure 2 Transmission electron micrographs of WS_2/SiO_2 composite. (a) A typical region showing several WS_2 needles. (b) HRTEM of a single WS_2 crystal, showing lattice fringes along the (0 0 2) plane. (c) A large WS_2 crystal exhibiting folding and other geometric deformations. (d) Electron diffraction pattern of the crystal in (c), showing spots due to (h, k, 0) reflections.

TABLE I X-ray powder diffraction data for SiO_2 nanocomposites

Guest	d (nm)/(h, k, l)					$W_{1/2}$ of indicated peak 2θ (deg)
WS_2	0.272 (1,0,0)	0.267 (1,0,1)	0.158 (1,1,0)			1.0 (d = 2.7)
δ-WN	0.206	0.145 (1,1,0)	0.251 (1,0,0)			4.5 (d = 1.5)
Fe_3O_4	0.253 (3,1,1)	0.149 (4,4,0)	0.209 (4,0,0)	0.160 (5,1,1)	0.296 (2,2,0)	1.2 (d = 2.5)
Fe_9S_{10}	0.207 (8,6,6)	0.172 (11,9,0)	0.266 (7,6,0)	0.159 (15,6,0)	0.144 (17,6,1)	0.8 (d = 2.1)

The reaction of tungsten-filled silica aerogel with anhydrous ammonia at 480 °C produced a composite of δ-WN and SiO_2. Carrying out this process above 550 °C led to the absence of tungsten-containing products. This probably resulted from reaction of the silica surface with NH_3 [18]. Liberated water could then react with any δ-WN, forming more volatile WO_x products. Fig. 3 shows an electron micrograph of the δ-WN/SiO_2 composite. The material contains δ-WN particles ranging from 1–5 nm. The small particle sizes

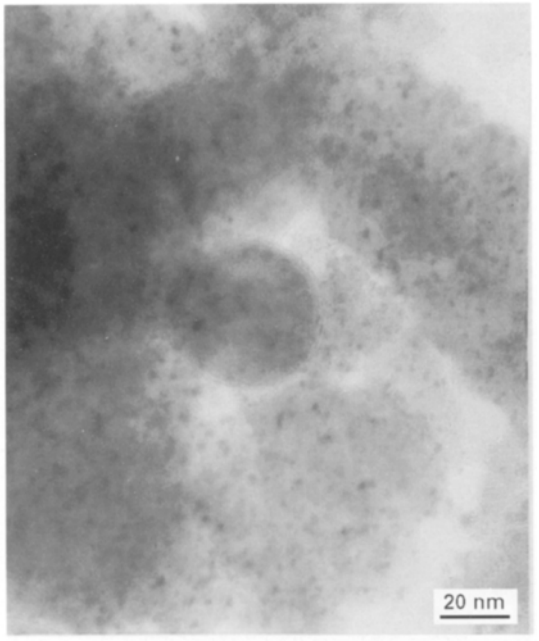

Figure 3 HRTEM micrograph of the δ-WN/SiO_2 aerogel nanocomposite. Severe radiation damage by the electron beam did not permit finer resolution.

in this composite agree with the broad, weak peaks seen in the powder XRD patterns. The δ-WN crystals in this sample showed significant radiation damage during electron microscopy, making imaging of a single crystal, or EDS analyses, unreliable.

The deposition of $Fe(CO)_5$ in silica aerogel required caution, owing to the higher vapour pressure of adsorbate. $Fe(CO)_5$ readily fills the pores of the aerogel host, to the extent that the surface tension of the liquid phase causes collapse of the macropores of the host. The resulting material loses its structural integrity and transforms into a powder. Additional cautions arise from the pyrophoric nature of $Fe(CO)_5$-filled aerogel. Rapid exposure to air results in spontaneous ignition, producing a dense material that visibly appears to contain several FeO_x species. Careful reaction with air led to an orange–brown product that appeared amorphous in electron microscopy, but probably contained Fe_2O_3 and FeO(OH). Further addition of $Fe(CO)_5$ to this material does not lead to additional Fe_2O_3, but rather Fe_3O_4, possibly according to the reaction

$$4Fe_2O_3 + Fe(CO)_5 \rightarrow 4Fe_2O_3 + Fe + 5CO \rightarrow 3Fe_3O_4 + 5CO \quad (2)$$

The composite as prepared initially, showed a slight attraction to a magnet. Annealing the composite at 720 °C under 50% argon/air significantly increased the magnetism of the material. However, this also lead to shrinkage and cracking of the gel. The *B*–*H* curve of the annealed Fe_3O_4/SiO_2 aerogel composite is shown in Fig. 4, where *B* is the magnetic flux and *H* is the magnetic field strength. The composite exhibits soft ferromagnetic behaviour, with a coercive force of ~170 Oe. Electron micrographs of the composite show particles of Fe_3O_4 ranging from 20 –55 nm (mean 36 nm, S.D. = 7 nm) (Fig. 5). XRD did not reveal crystalline phases other than Fe_3O_4.

Passing H_2S vapours over a piece of Fe_2O_3/FeO(OH)-filled silica aerogel at 900 °C lead to the formation of the unusual phase Fe_9S_{10}, as determined by XRD. Lower reaction temperatures resulted in amorphous products that decomposed over prolonged exposure to air. The high-temperature reaction, as above, caused significant shrinkage and cracking of the sample. However, stable, crystalline Fe_9S_{10} also formed with particle sizes ranging from 30–90 nm (mean 48 nm, S.D. = 10 nm) as shown in Fig. 6. Diffraction patterns for FeS or FeS_2 did not appear in the XRD analysis of the Fe_9S_{10}/SiO_2 composite. These phases could probably be produced by varying the sulphur source or other reaction conditions.

It is notable that shrinkage and densification occurred only for the samples that contained iron and were

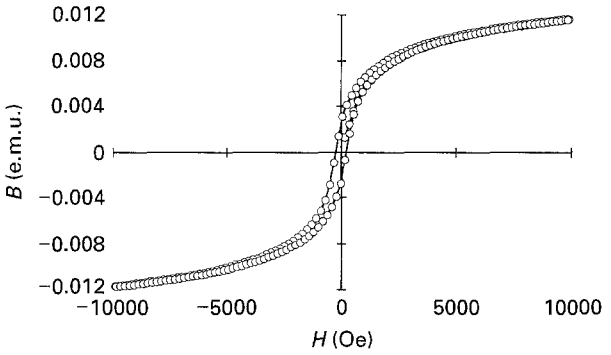

Figure 4 *B*–*H* curve of the Fe_3O_4/SiO_2 nanocomposite.

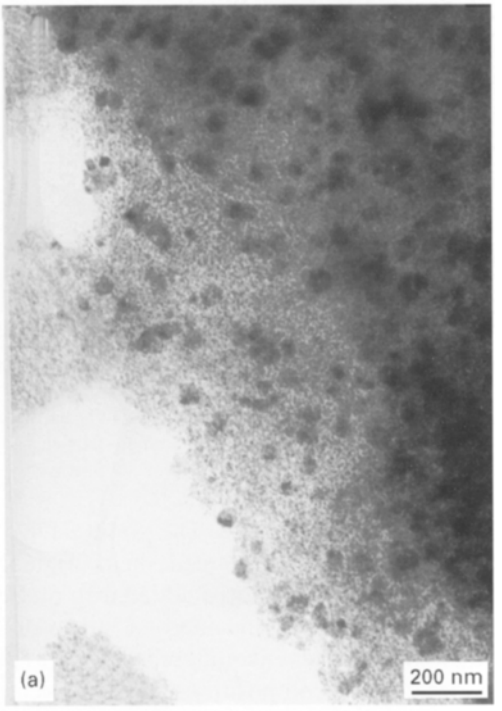

Figure 5 Electron micrographs of the Fe_3O_4/SiO_2 nanocomposite. (a) Low-magnification image showing numerous magnetite particles. (b) HRTEM of single-domain magnetite particles, the top particle shows lattice fringes along the (2 2 0) plane while the bottom particle shows fringes along the (2 2 2) plane. (c) Electron diffraction pattern showing the (*xxx*) ring.

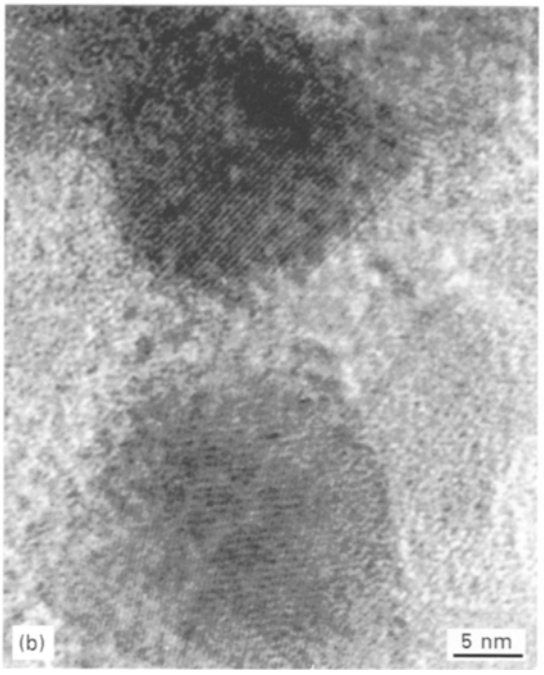

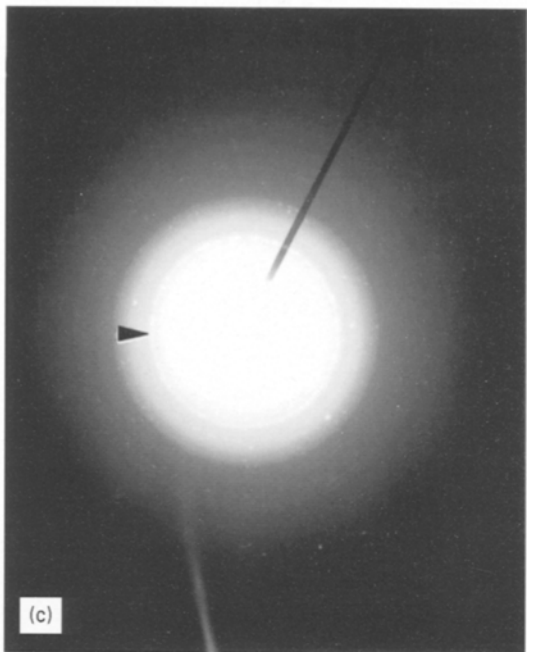

Figure 5 Continued

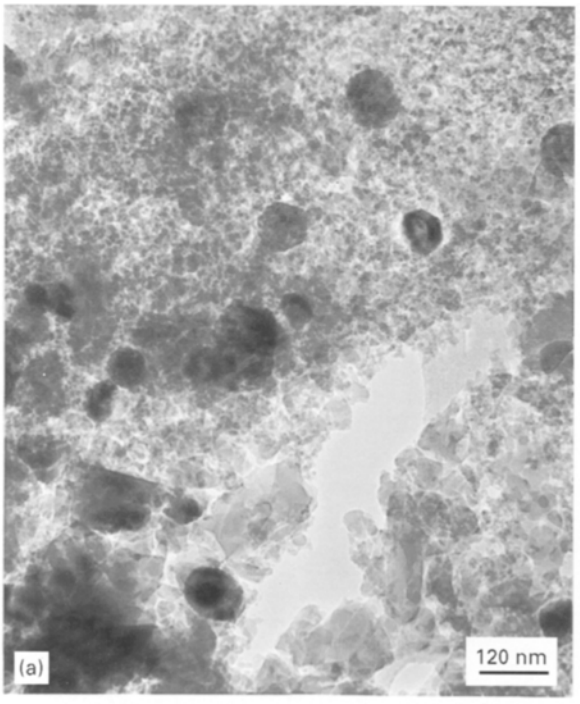

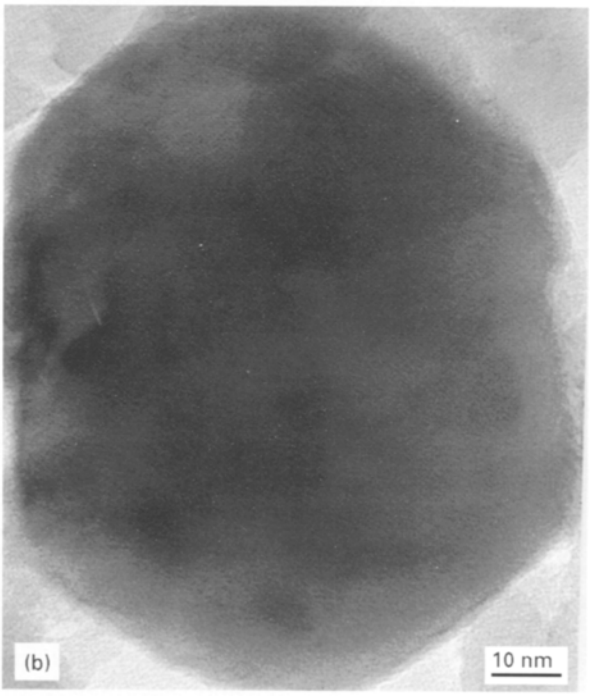

Figure 6 Electron micrographs of the Fe_9S_{10}/SiO_2 nanocomposite. (a) Image showing several Fe_9S_{10} particles; sintered SiO_2 formed at 900 °C can also be seen. (b) HRTEM of a single particle. Lattice images of this material quickly degraded in the electron beam; however, residual fringes can be seen near the edge of the particle.

expoded to high temperatures. The samples filled with tungsten compounds maintained their original size and density. It is likely that the added iron phases act as sintering aids for the silica aerogel substrate. This phenomenon may be encountered when preparing composites of other compositions, and should be considered when low-density materials are desired.

4. Conclusions

Nanocomposite materials with silica aerogel as the host matrix are simply prepared using chemical vapour infiltration/decomposition methods. $W(CO)_6$ and $Fe(CO)_5$ both deposit easily in the host material. Thermal treatment of the $W(CO)_6$-filled aerogel forms an amorphous tungsten phase within the aerogel. Treatment of this material with sulphur gives WS_2/silica aerogel nanocomposites, while treatment with NH_3, gives a similar composite containing δ-WN. Silica aerogel filled with $Fe(CO)_5$ is more conveniently oxidized to an amorphous iron oxide/silica aerogel composite. This can then be reacted with additional $Fe(CO)_5$ to give a magnetic composite of Fe_3O_4, or with H_2S to give a composite containing

Fe_9S_{10}. Guest-phase particle sizes ranged from 1–90 nm. Careful manipulation of the experimental conditions should allow for the preparation of various guest-phase dimensions to meet specific applications requirements.

Acknowledgements

The authors thank the National Center for Electron Microscopy at Lawrence Berkeley Laboratory for providing electron microscopy facilities, and the group of Professor Gareth Thomas, University of California, Berkeley, for the use of their vibrating sample magnetometer. This work was supported by the Assistant Secretary for Energy Efficiency and Renewable Energy, Advanced Industrial Materials Program, Office of Industrial Technologies of the US Department of Energy under Contract DE-AC03-76SF00098.

References

1. G. D. STUCKY and J. E. MAC DOUGAL, *Science* **247** (1990) 669.
2. T. SHINJO, *J. Phys. Soc. Jpn* **21** (1966) 327.
3. B. RODMACQ, *J. Phys. Chem. Solids* **45** (1984) 1119.
4. J. Q. WANG, P. XIONG and G. XIAO, *Phys. Rev. B Condens. Matter* **47** (1993) 8341.
5. V. R. PRADHAN, J. W. TIERNEY, I. WENDER and G. P. HUFFMAN, *Fuels* **5** (1991) 497.
6. T. OSAKI, H. TAODA, T. HORIUCHI and H. YAMAKITA, *React. Kinet. Catal. Lett.* **51** (1993) 39.
7. A. TROVARELLI, P. MATTEAZZI, G. DOLCETI and A. LUTMAN, *Appl. Catal. A Gen.* **95** (1993) L9.
8. B. BREITSCHEIDEL, J. ZIEDER and U. SCHUBERT, *Chem. Mater.* **3** (1991) 559.
9. C. M. LUKEHART, J. P. CARPENTER, S. B. MILNE and K. J. BURNHAM, *CHEMTECH* August (1993) 29.
10. P. H. TEWARI, A. J. HUNT and K. D. LOFFTUS, *Mater. Lett.* **3** (1985) 363.
11. JCPDS "Powder Diffraction File" (International Center for Diffraction Data, Swarthmore, PA, 1988).
12. C. J. BRINKER and G. W. SCHERER, "Sol-Gel Science" (Academic Press, San Diego, 1990).
13. A. W. ADAMSON, "Physical Chemistry of Surfaces", 5th Edn (Wiley, New York, 1990)
14. H. DAAMEN, J. M. ERNSTING and A. OSKAM, *Thermochim. Acta* **33** (1979) 217.
15. A. G. GILBERT and K. G. P. SULZMANN, *J. Electrochem. Soc.* **121** (1993) 386.
16. R. TENNE, L. MARGULIS and G. HODES, *Adv. Mater.* **5** (1993) 386.
17. R. TENNE, L. MARGULIS, M. GENUT and G. HODES, *Nature* **360** (1992) 444.
18. P. FINK, B. MULLER and G. RUDAKOFF, *J. Non-Cryst. Solids* **145** (1992) 99.

Received 7 June 1995
and accepted 2 July 1996